# Development of Mercury Analysis by NanoSIMS for the Localization of Mercury–Selenium Particles in Whale Liver

Dirk Schaumlöffel, Maria Angels Subirana, Lhiam Paton, James Hall, Andrew Brownlow, Eva M Krupp, Jörg Feldmann, Maria Angels Subirana

# Development of mercury analysis by NanoSIMS for the localization of mercury-selenium particles in whale liver

Maria Angels Subirana[1], Lhiam Paton[2], James Hall[3], Andrew Brownlow[4], Eva M. Krupp[3], Jörg Feldmann[2] and Dirk Schaumlöffel[1*]

[1]CNRS, Université de Pau et des Pays de l'Adour, E2S UPPA, Institut des Sciences Analytiques et de Physico-Chimie pour l'Environnement et les Matériaux, UMR 5254, 64000 Pau, France

[2]TESLA-Analytical Chemistry, Institute of Chemistry, University of Graz, 8010 Graz, Austria

[3]TESLA- Chemistry, School of Computing and Physical Sciences, University of Aberdeen, Aberdeen, AB24 3UE, Scotland, UK

[4]Marine Animal Stranding Scheme, Institute of Biodiversity, Animal Health & Comparative Medicine, College of Medical, Veterinary & Life Sciences, University of Glasgow, Glasgow, G12 8QQ, Scotland, UK

*Corresponding author:
Dirk Schaumlöffel
CNRS, Université de Pau et des Pays de l'Adour, E2S UPPA, Institut des Sciences Analytiques et de Physico-Chimie pour l'Environnement et les Matériaux (IPREM) UMR 5254, Hélioparc, 2 av. du président Angot, 64053 Pau, France
Tel.: +33-559-407760; Fax: +33-559-407674
E-mail address: dirk.schaumloeffel@univ-pau.fr

**ABSTRACT**

Nanoscale secondary ion mass spectrometry (NanoSIMS) is a dynamic SIMS technique, which offers high spatial resolution allowing the mapping of chemical elements at the nanometer scale combined with high sensitivity. However, SIMS for mercury analysis is a challenging issue due to the low secondary ion yield and has never been done on NanoSIMS. The introduction of an rf plasma oxygen primary ion source on NanoSIMS enabled higher lateral resolution and higher sensitivity for electropositive elements such as most metals. In this paper, for the first time mercury analysis by NanoSIMS was developed applying the new rf plasma $O^-$ ion source. All mercury isotopes could be detected as $Hg^+$ secondary ions and the isotopic pattern corresponded to their natural isotopic abundances. Furthermore, $Hg^+$ detection in HgSe nanocrystals has been investigated where polyatomic interferences from selenium clusters were identified and separated by high mass resolution ($\Delta M/M \geq 3200$). However, in presence of selenium a strong matrix effect was observed decreasing the $Hg^+$ secondary ion yield. In addition, a detection of $Se^+$ ions was possible, too. The newly developed method was successfully applied to nanoscale localization by chemical imaging of HgSe particles accumulated in liver tissue of sperm whale (*Physeter macrocephalus*). This demonstrated the applicability of NanoSIMS not only for mercury detection in surface analysis but also for mercury mapping in biological samples.

Key words:

NanoSIMS, mercury, selenium, rf plasma oxygen ion source, whale liver

## Introduction

Mercury and mercury compounds have been used in industrial processes, in electric and electronic applications as well as in medicine [1]. Due to considerable emissions by anthropogenic and natural sources, mercury has been identified as global toxic pollutant that can bioaccumulate and biomagnify in organisms through the trophic chain [2,3]. Therefore, it is essential to monitor the use, global distribution and toxicity of mercury requiring powerful techniques for mercury analysis in all kind of materials. Secondary ion mass spectrometry (SIMS) is an important analytical technique for surface characterization, depth profiling or chemical imaging of solid matter; however, SIMS for mercury analysis is challenging

In SIMS a focused positive or negative primary ion beam sputters a sample surface and generates secondary ions, which are collected and subsequently analyzed by a mass spectrometer [4]. A combination of a low energy, pulsed ion beam (e.g. $Ga^+$, $Bi^+$, and $Bi_3^+$) with, usually, a time-of-flight (ToF) mass spectrometer belongs to the static SIMS technique which allows the generation of elemental and molecular secondary ions of the topmost atomic layer of a surface [5]. The dynamic SIMS technique uses a high-energy ion beam of either cesium ($Cs^+$) or oxygen ($O_2^+$ or $O^-$) ions that generate elemental secondary ions from several atomic layers, which are analyzed by a sector field mass spectrometer [6].

In general, the detection limit of the SIMS technique can go down to the tens of parts per billion. However, the actual detection will be determined by the generation of secondary ions from the sample. This is influenced by several factors: i) the atomic density of the analyte in the sample, ii) the composition of the matrix, iii) the sputtering rate of the analyte from the surface by the primary beam, iv) the ionization of those sputtered atoms (ion yield), and v) the transmission of those ions to the detector [7]. The main limiting factor in SIMS, other than the actual sample concentration, is the variability in the ion yield between elements [8]. This ion yield is

proportional to either the electron affinity, for negative secondary ions, or the ionization energy, for positive ions [4].

In the case of mercury, Storms *et al.* [9] described $Hg^-$ as barely detectable when using a $Cs^+$ ion source. With an $O^-$ primary ion source $Hg^+$ secondary ions could be obtained, however, with an ion yield three orders of magnitude lower than those of other metals such as Ca, Mg or Fe. Consequently, to date, only a few studies have analyzed mercury by SIMS due to this low secondary ion yield observed, as follows. Dynamic SIMS with $O_2^+$ and $Cs^+$ sources has been applied so far only for depth profiling of mercury in semiconductors [10,11], electrical sensors [12], membranes [13], electrodes [14] or for investigating steel corrosion [15]. The few examples applying static SIMS for detection of elemental and molecular mercury ions encompass surface analysis and depth profiling of semiconductors [16], characterization of mercury amine ions on surfaces [17], detection of mercury thiolate ions in self-assembling monolayers [18], and depth profiling of methylmercury species in air-dried layers of bacteria [19]. Only two publications describe the use of ToF-SIMS for chemical imaging of mercury. One study clarified the darkening process (photodegradation) of the red pigment vermilion (red mercury sulfide) in paintings via detection of Hg-S-Cl cluster ions in small sample areas [20]. Another ToF-SIMS study investigated the spatial distribution of mercury and other elements in cholesterol gallstones [21]; however, the detection of $Hg^+$ secondary ions was very weak and resulted in only low-resolved images.

So far, mercury analysis by nanoscale secondary ion mass spectrometry (NanoSIMS) has never been described in the scientific literature. NanoSIMS is a dynamic SIMS technique characterized by its high spatial resolution. This is accomplished due to the perpendicular focusing of the positive ($Cs^+$) or negative ($O^-$) primary ion beam to the sample surface allowing chemical and isotopic imaging with high spatial resolution combined with high sensitivity. The required narrow focusing of the ion beam is achieved by using ion sources that provide high beam current densities and low beam energy dispersion. Since the introduction of the

instrument, the $Cs^+$ ion source on NanoSIMS has been able to achieve 50-nm-resolution images of electronegative elements such as carbon, nitrogen, oxygen, and sulfur. However, only the recent introduction of an rf plasma oxygen primary ion source on NanoSIMS allowed high lateral resolution down to 40 nm and high sensitive detection of electropositive elements such as most metals, which opens numerous new research possibilities [22].

The aim of this study was to develop mercury analysis by NanoSIMS by the application of an rf plasma $O^-$ primary ion source to biological samples, which are known to contain HgSe clusters as natural nanoparticles [23,24]. Firstly, $Hg^+$ detection in HgSe nanocrystals has been investigated where interferences from selenium clusters were identified and separated by high mass resolution. The newly developed method was successfully applied to nanoscale localization by chemical imaging of HgSe particles accumulated in liver tissue of sperm whale (*Physeter macrocephalus*). We aimed to demonstrate the applicability of NanoSIMS as a tool for Hg analysis in environmental science, biology, and toxicology, where low Hg concentrations can be found.

## Experimental section

*Preparation of standards and nanocrystalline HgSe*

Elemental standards of mercury, selenium, and sodium were prepared by slow evaporation at room temperature of a drop of standard solutions of Hg, Se and Na in $HNO_3$ at a 1000 µg/ml concentration (PlasmaCAL, SPC Science, Canada) on a silicon wafer.

Nanocrystalline HgSe was synthesised following the method described by Kristl and Drofenik [25] by the reaction of mercury nitrate and selenium powder. Briefly, 0.474 g (0.006 mol) of selenium powder (99+ %, Alfa Aesar) was dissolved in 50 mL of 5M NaOH solution, assisted with sonication, and mixed with a solution of 1.713 g (0.005 mol) $Hg(NO_3)_2.H_2O$ (99.99+ %, Sigma Aldrich, UK) dissolved in 0.1 M EDTA. The molar ratio of 1:1.2 (Hg:Se) was advised

as an alternative to performing the reaction under nitrogen flow. The mixture was sonicated at room temperature as the addition of the mercury solution to the alkaline selenium solution occurred, and after 15 minutes of sonication the reaction was continued on a hot plate at approximately 80 °C for 30 minutes. The solution was then cooled and washed with EDTA to remove cations including additional $Hg^{2+}$, water and ethanol. The solution was deposited on a silicon wafer and evaporated.

*Whale sampling*

Samples from a sperm whale *(Physeter macrocephalus)* were provided by the Scottish Marine Animal Stranding Scheme (SMASS). The sub-adult male sperm whale was stranded and sampled at Ardersier, Scotland (Latitude: 57.5626, Longitude: -4.04194). The whale was sampled soon after death. Reports on the stranding can be found on the SMASS website (Scottish Marine Aimals Stranding Scheme: https:\\stranding.org accessed 22 June 2021). Sections of whale liver were taken from the whale and stored at 4 °C prior to preparation for NanoSIMS 12 hours later. The parts of the tissue were randomly selected as previous studies indicate that that Hg and Se were heterogenously distributed throughout the whale liver tissue and each area of the liver looked similar as far as Hg and Se distribution[24].

*Preparation of whale samples for NanoSIMS*

Sample preparation was performed at the Microscopy and Histology Core Facility at the Institute for Medical Sciences, Aberdeen, UK. 4 mm diameter discs of tissue were transferred into gold-plated copper specimen carriers filled with hexadecane. Extracted tissue samples were flash frozen under high pressure using a Leica EM ICE (Leica Microsystems, Milton Keynes, UK). Automatic freeze substitution with 2% osmium tetroxide ($OsO_4$) in acetone was carried out using a Leica AFS 2 (Leica Mircosystems, Milton Keynes, UK), followed by

embedding in Spurr's resin (TAAB, UK) and acetone. Finally, the samples were polymerized at 60 °C for 24 hours. Sections of 300 nm were cut from the resin block using a diamond knife (Diatome Ltd, Switzerland) on an ultra-microtome (Leica UC6, Leica Microsystems) and placed on silicon wafers (Ted Pella, USA) for NanoSIMS analysis.

*Detection of stable mercury isotopes by NanoSIMS*

Nanoscale secondary ion mass spectrometry analysis was performed using the NanoSIMS 50L (Cameca, Gennevilliers, France) equipped with the Hyperion rf plasma primary oxygen ion source (Oregon Physics, Beaverton, USA). A primary $O^-$ beam of approximately 200 nA was used. The isotopic distribution of Hg was investigated in the mercury standard and the nanocrystalline HgSe to identify the corresponding isotopes as well as possible interferences for each mass. The isotopes of mercury were recorded in an electron multiplier detector by scanning the magnetic field (B field scan) from 2673.123 G to 2807.307 G (equivalent to masses 194 to 214) with 0.37 G steps, resulting in 364 points with 1 s counting time per point and a mass resolution of approximately 2500, using an $O^-$ beam of 75 pA on the sample (D1=2). The entrance (ES) and aperture slits (AS) were opened fully to allow maximum transmission of the ions to the detectors considering the very low yield expected for Hg.

Theoretical simulation of the resulting mass spectra for the HgSe standard was performed with the online tool Mass Spectrum Simulator from Prot pi (developed by the Zurich University of Applied Sciences). In order to match the experimental spectrum, the following compounds were considered to contribute to the mass spectrum between 194-214: $Hg^+$, $Se_2NO_2^+$, $SeH_5O_7^+$, $NaSeNO_5^+$, with a relative intensity ratio set at 0.01, 0.6, 0.5 and 0.5 respectively, and a mass resolution of 2500. The same calculation was also performed for Hg to compare with the experimental spectrum of the Hg standard.

High resolution mass spectra of the selected $^{198}Hg$ and $^{202}Hg$ isotopes were recorded in two detectors by scanning the voltage applied to each, from 12 V to 55 V with 0.51 steps in 110 points, with a counting time of 0.76 s per point, using an $O^-$ beam of 34 pA in the sample (D1=3, open ES and AS slits), which resulted in a mass resolution of approximately 3200 with the required optimization. With this resolution, it was possible to distinguish the Hg signal from that of the interferences, and the mass spectrometer was calibrated to record the Hg isotopes excluding any signal coming from the interferences. Technical reasons of the NanoSIMS instrument required a minimal distance of 4 amu between two detectors at these high masses.

*NanoSIMS imaging*

The elemental Hg standard and the nanocrystalline HgSe were mapped using the 200 nA $O^-$ beam, in order to observe the distribution of $^{80}Se$, $^{198}Hg$ and $^{202}Hg$ isotopes, by analysing an area of 25x25 µm in the surface with 256x256 pixels and 10 ms of dwell time per pixel with an $O^-$ beam of 38 pA in the sample (D1=3, open ES and AS slits). Seven subsequent analyses were performed in the same area, during 1 hour and 16 minutes, and later accumulated with the WinImage software (Cameca, France), to increase the signal to noise ratio.

Gold coating of the sample surface with a 5 nm Au layer in order to increase conductivity and ion yield was attempted using a 108 auto sputter coater equipped with a thickness monitor (Cressington, UK).

The liver tissue of the sperm whale was mapped, too. Areas were selected from optical images (Figure S-1) in which darker spots were seen to indicate HgSe agglomerations, obtained with the CCD camera from the NanoSIMS instrument. The isotopes $^{12}C$, $^{23}Na$, $^{80}Se$, $^{198}Hg$ and $^{202}Hg$ were measured simultaneously. Images of 30x30 and 35x35 µm were acquired with 256x256 pixels and 10 ms of dwell time per pixel with an $O^-$ beam of 10 pA in the sample. The same area was measured during 18 hours, accumulating 100 planes with WinImage. Consistent signal

intensity throughout the planes for all measured isotopes, including constant signal intensity of $^{12}C^+$ ions obtained from the resin matrix, indicated that the sample was not consumed completely during the long acquisition time. Beam size was calculated with the knife-edge method (16-84% principle) [22].

## Results and discussion

*Detection of mercury isotopes from a mercury standard*

The mass spectrum of secondary $Hg^+$ ions obtained from a mercury standard sputtered with an $O^-$ ion beam is shown in Figure 1a. The maximum count rate was about $10^3$ cps for the most abundant $^{202}Hg$ isotope while the background was close to 0 cps. All natural stable mercury isotopes were detected with an isotopic pattern reflecting their natural abundance, which was well in agreement with the theoretical simulation (Figure 1a). In addition, the detection of $HgO^+$ ions was tested as suggested by Zalavutdinov et al [15]. In our experiments we could observe $HgO^+$ secondary ions, however, the ion yield was about 20 times lower than for the respective $Hg^+$ ion. This is in agreement with the observations of Storms and co-workers [9] who showed, for all metals sputtered with an $O^-$ beam, a lower ion yield for $MO^+$ ions than for the $M^+$ ions. The diatomic isotope $Hg_2^+$ was also screened but was barely detected.

Two mercury isotopes, $^{198}Hg$ and $^{202}Hg$, were chosen for further analysis. High-resolution mass spectra were recorded (Figures 1c and d) and the mass spectrometer calibrated for the exact masses of the isotopes. Then an elemental image of the isotopes $^{198}Hg$ and $^{202}Hg$ was obtained from the elemental Hg standard where the two mercury isotopes showed a perfect overlay (Figure 2).

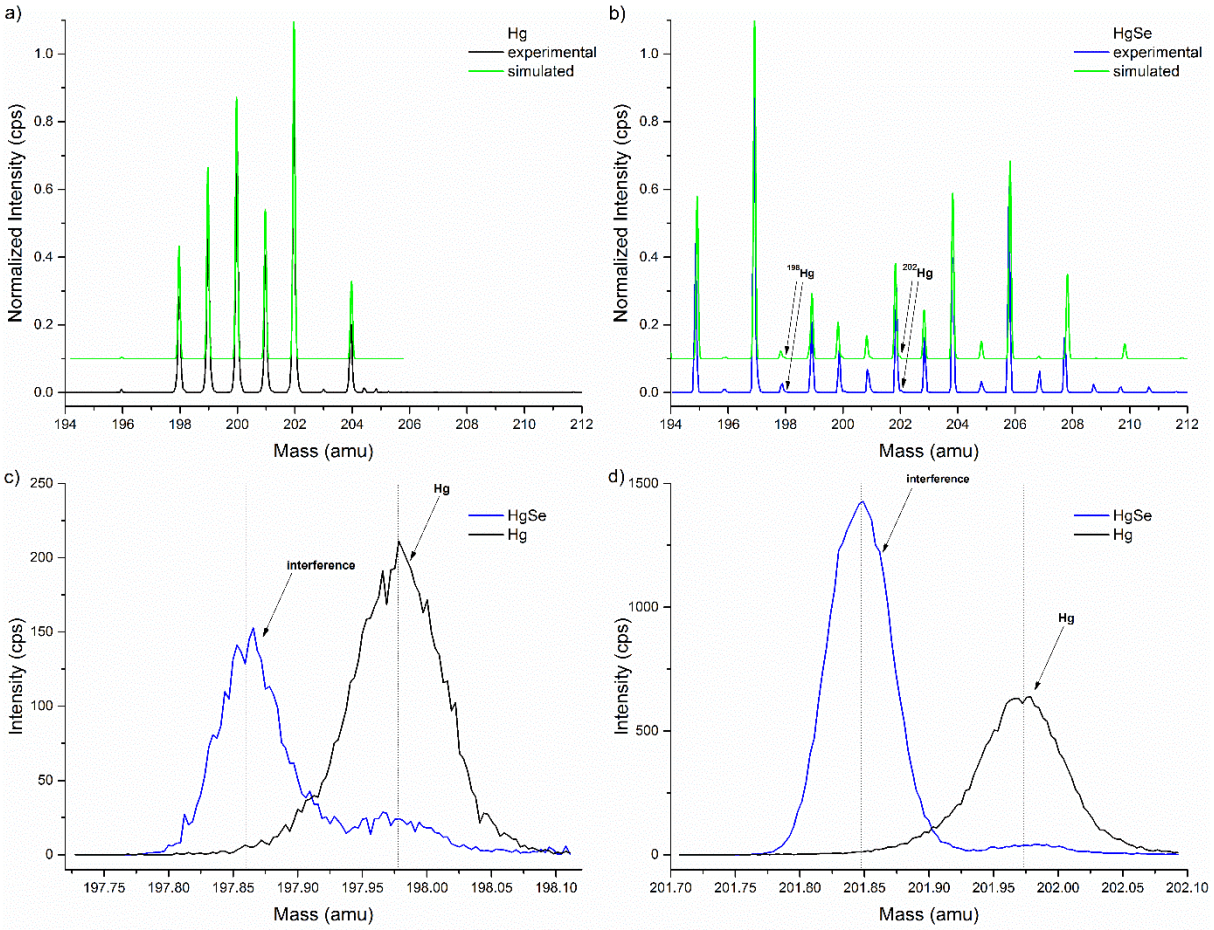


*Figure 1: a) Mass spectrum obtained by a magnetic field scan from a mercury standard (black) and theoretical simulation of the isotopic pattern of Hg (green, offset), b) mass spectrum obtained by a magnetic field scan from nanocrystalline HgSe (blue) and theoretical simulation of the combination of Hg isotopes with $Se_2NO_2^+$, $SeH_5O_7^+$, and $NaSeNO_5^+$ interferences (green, offset), Small Hg peaks appeared for $^{198}Hg$ and $^{202}Hg$ (arrows). c) high resolution mass spectra from mass 197.73 to 198.12 from the mercury standard ($^{198}Hg$ detection, black) and the nanocrystalline HgSe (blue) and d) high resolution mass spectra from mass 201.71 to 202.10 obtained from the Hg standard ($^{202}Hg$ detection, black) and HgSe (blue).*

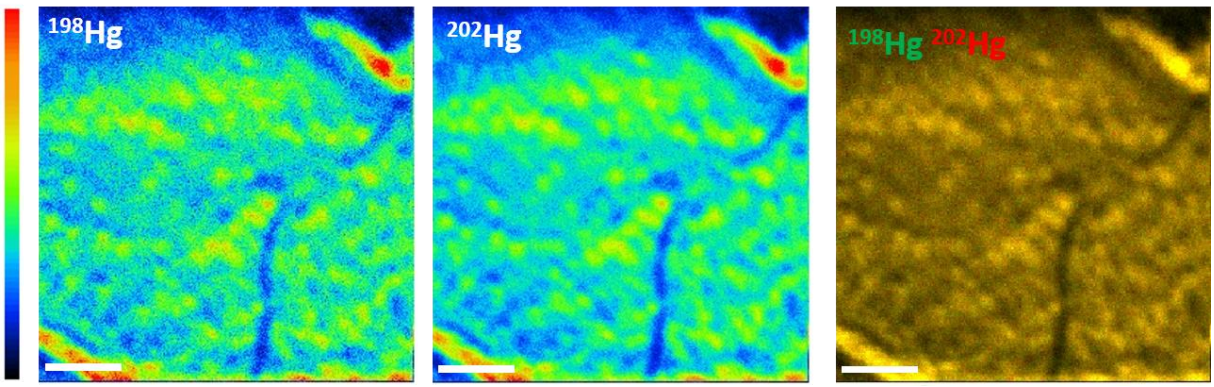


*Figure 2: Mapping in a Hg standard of $^{198}Hg$ and $^{202}Hg$, color overlay of $^{198}Hg$ (green) and $^{202}Hg$ (red). Color scale on the top left indicates relative intensity in counts per second in each image, which ranges from: $^{198}Hg$ 0 to 120 cps, $^{202}Hg$ 0 to 350 cps. Scale bar is 5 µm.*

*Detection of mercury in nanocrystalline HgSe powder*

Synthesized nanocrystalline HgSe powder on a silicon wafer was sputtered with an $O^-$ ion beam and the mass spectrum, of the resulting secondary $Hg^+$ ions, was registered with a B field scan (Figure 1b). The mass spectrum shows interfering mass peaks close to the Hg isotope peaks. The interferences are most likely different clusters of the elements H, N, O, Na, and Se which are present in the sample according to the HgSe powder synthesis protocol. A simulated mass spectrum of three potential clusters (Figure 1b) is in agreement with the spectrum of the sample suggesting a combination of interferences from $SeH_5O_7^+$, $NaSeNO_5^+$, and $Se_2NO_2^+$ cluster ions, the latter being the most important interference in the mass range of the mercury isotopes.

Furthermore, Figure 1b indicates that the interference peaks do not overlap completely with the peaks of the mercury isotopes at a mass resolution ≥2500, but that the $^{198}Hg$ and $^{202}Hg$ signals appear as small peaks, at a 0.12 amu higher mass, in the mass spectrum. Subsequently recorded high mass resolution spectra ($\Delta M/M \geq 3200$) at m/z 198 and 202 show a clear separation of the $Hg^+$ signal from the interference. The intensity of the $Hg^+$ signal obtained from nanocrystalline

HgSe is much lower than that obtained from the mercury standard, analyzed under the same instrumental conditions indicating a strong matrix effect, which suppress the Hg ionization in presence of selenium. This is in agreement with the literature that describe a strong dependence of the secondary ion yield in SIMS from the sample matrix [26], which renders quantitative analysis difficult. Other possible isotopes such as $HgSe^+$ and $HgSeO^+$ were tested for mercury detection in HgSe but resulted in even lower ion yields.

After precise mass calibration of the detectors for the ions $^{80}Se$, $^{198}Hg$, and $^{202}Hg$, an elemental image of nanocrystalline HgSe powder was recorded (Figure 3). It shows clearly a colocalization of these three elements demonstrating that an imaging of HgSe particles is possible with correct detection of mercury and selenium. Note, that a detection of $^{80}Se^+$ ions was possible in nanocrystalline HgSe with an ion yield of about 25 times higher than of $^{202}Hg^+$, enabling a parallel analysis of mercury and selenium.

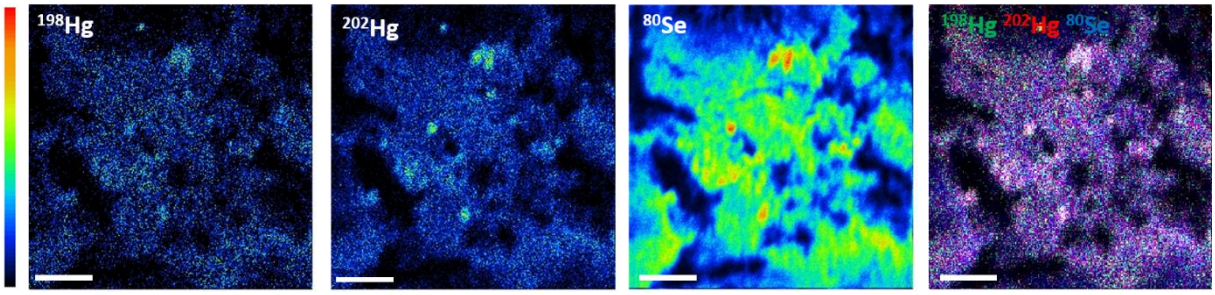


*Figure 3: Mapping in a nanocrystalline HgSe standard of $^{198}Hg$, $^{202}Hg$, and $^{80}Se$, color overlay of $^{198}Hg$ (green) and $^{202}Hg$ (red) and color overlay of $^{202}Hg$ (red) and $^{80}Se$ (blue). Color scale on the top left indicates relative intensity in counts per second in each image, which ranges from: $^{198}Hg$ 0 to 7 cps, $^{202}Hg$ 0 to 15 cps, $^{80}Se$ 0 to 370 cps. Scale bar is 5 µm.*

*Gold coating of the sample surface*

Depending on the sample, gold coating of the sample surface may be necessary for SIMS analysis in order to ensure a conductive surface [27], and furthermore, gold coating can enhance the secondary ion yield in some cases [28]. Therefore, the influence of gold coating on mercury analysis in NanoSIMS was evaluated. Both, the mercury standard and the nanocrystalline HgSe powder were coated with a 5-nm gold layer with help of a sputter coater and mass spectra were recorded by a B field scan (entire spectrum) and voltage scan (high resolution spectra), respectively. Beside the additional peak of $^{197}$Au no additional interferences were detected (Figure S-2a). Moreover, high resolution spectra revealed that gold coating suppressed the mercury secondary ion yield by 30 to 50 % (Figure S-2b). It can be concluded that a gold coating can be applied, if necessary, in order to ensure sample surface conductivity, but did not shows positive effects on the ion yield. Therefore, in our further experiments a gold coating was not applied.

*Detection of HgSe particles in whale liver tissue*

The developed NanoSIMS method for mercury analysis was applied to the localization of HgSe particles in liver tissue from sperm whale. Images of 30-35 µm x 30-35 µm were recorded with simultaneous detection of $^{23}$Na, $^{80}$Se, $^{198}$Hg, and $^{202}$Hg (Figure 4), using a beam of 100nm diameter.

Aggregations of >50 particles were observed containing both Hg and Se. Here, the signal intensity for $^{80}Se^{+}$ ions was in the same order of magnitude than for $^{202}Hg^{+}$. Na was used to image the structures in the whale tissue, and suggests particles contain less Na compared to surrounding organic material. Basing on line scans through the particles images obtained from NanoSIMS measurements (Figure S-3), the particle size was roughly estimated. The aggregates

had a size of around 10-30 µm, containing particles with a size of approximately 400 to 550 nm, which agglomerated in small clusters of few particles that ranged from 1 to 2.5 µm. Additionally, both isotopes of mercury were detected in those nanoparticles, confirming unequivocally the identification of this toxic element. Mercury can accumulate in whale liver up to 500 mg $kg^{-1}$ dry weight [24], however, in this study a total Hg concentration of 86 mg $kg^{-1}$ dry weight was found (supporting information). Thus in our experiments the acquisition of about 100 single planes during 18 h measurement was necessary in order to sum up enough counts to achieve a sufficient mercury detection intensity that was significantly different to that in the background, especially for $^{198}Hg$. Accordingly, Hg imaging can be performed by NanoSIMS even at low bulk concentrations as long as the local concentration is sufficiently high. However, long acquisition times might be required for mercury imaging in biological samples.

The colocalization of these three isotopes indicated clearly the presence of HgSe particles in liver. Whales are on the upmost trophic level and bioaccumulate high concentration of metals via the food chain, including mercury [29]. The positive correlation of selenium and mercury content in cetacean tissue has been described before [30–32]. This led to the detection of inert HgSe particles in their organs, which endorse the hypothesis of the formation of this non-toxic Hg species as a mechanism of Hg tolerance and detoxification [29]. The results from our work are well in agreement with the two previous imaging studies of these particles in cetaceans. The first was accomplished in various organs of the striped dolphin (*Stenella coeruleoalba*) by using synchrotron-based X-ray fluorescence (XRF), but the low spatial resolution of a 1.5x1.5 µm beam only enabled the detection of aggregates of HgSe, which were estimated to be around 5 µm on an optical micrograph [33]. The second was performed in liver and brain of pilot whales (*Globicephala melas*), and employed laser ablation ICP-MS (with a 5x5 µm spot size) and XRF (2 $\mu m^2$ spot size) in order to image the particles in the whale tissue, and compensated the low

spatial resolution of both techniques with the use of single particle ICP-MS to estimate the particle size, which was found to be of 300-400 nm of average [24].

In the present study we show the first NanoSIMS imaging of mercury in a biological sample. The use of NanoSIMS technique surpassed the previous drawbacks of a low spatial resolution to demonstrate the accumulation of HgSe particles in whale liver at submicron level, with an unmatched combination of about 100 nm spatial resolution with high sensitivity, allowing the localization of particles of 400-550 nm in the tissue.

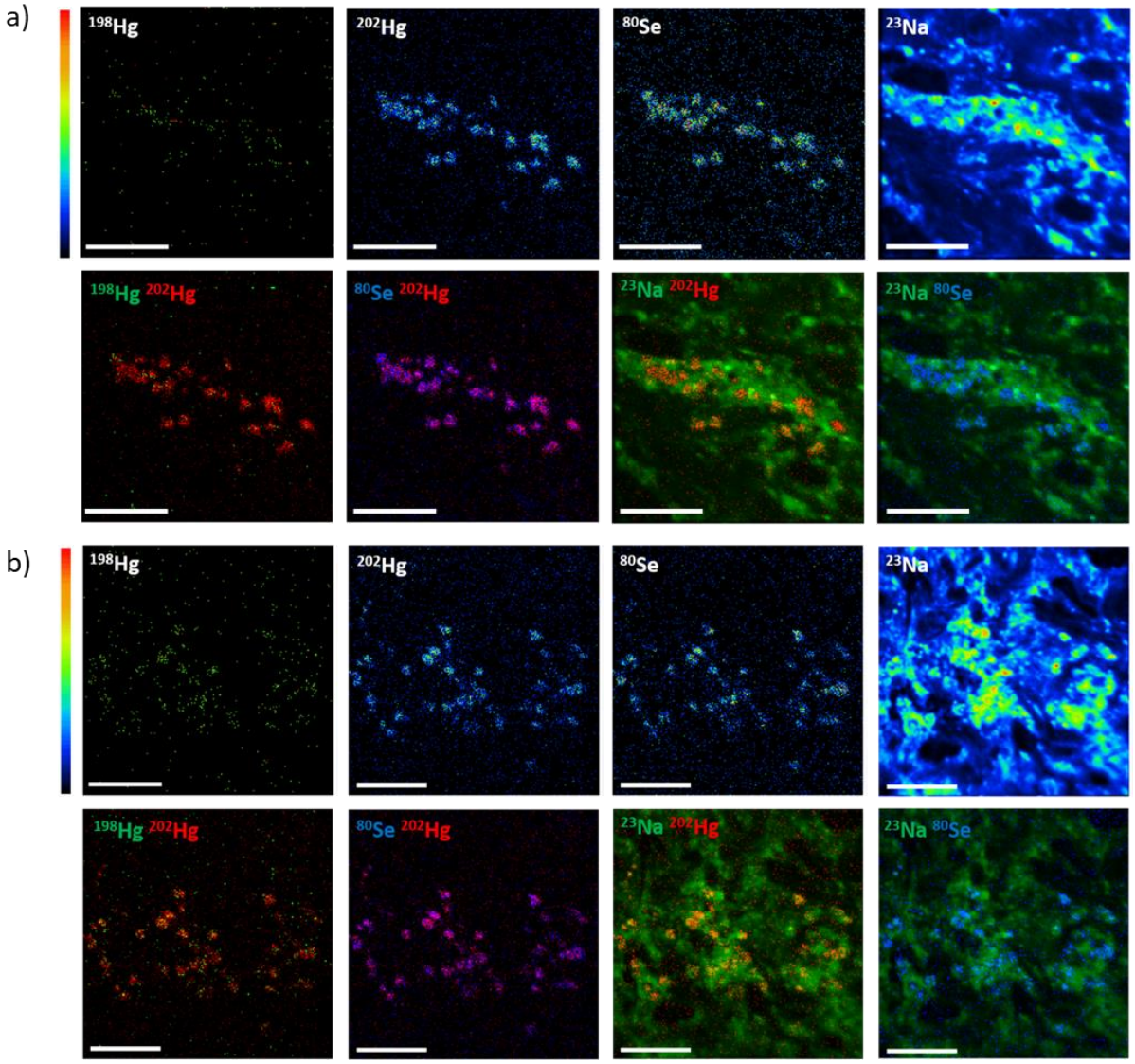


*Figure 4: Mapping of $^{198}Hg$, $^{202}Hg$, $^{80}Se$ and $^{23}Na$ in liver tissue. Two areas were analyzed: a) 30x30 µm and b) 35x35 µm. Color overlay of $^{198}Hg$ (green) and $^{202}Hg$ (red), color overlay of*

*$^{202}$Hg (red) and $^{80}$Se (blue), color overlay of $^{202}$Hg (red) and $^{23}$Na (green) and color overlay of $^{23}$Na (green) and $^{80}$Se (blue). Common color scale in the top left which ranges from: $^{198}$Hg 0 to 2 cps, $^{202}$Hg 0 to 6cps, $^{80}$Se 0 to 5 cp and $^{23}$Na 0 to 5000. Scale bar is 10 µm.*

## Conclusions

For the first time, a method for mercury detection in NanoSIMS was successfully developed owing to a new rf plasma oxygen primary ion source. All stable mercury isotopes could be detected. However, the secondary ion yield is strongly influenced by a matrix effect. Moreover, depending on the matrix, the presence of polyatomic interferences has to be carefully evaluated. For the analysis of HgSe particles all interferences were identified and separated by high mass resolution. NanoSIMS mercury imaging was applied for the first time to biological samples by localization of HgSe particles in whale liver tissue. A limitation is the long analysis time necessary for biological samples. While a submicrometer imaging of mercury containing particles is possible due to a higher local Hg concentration in the particles, a mercury analysis at trace levels seems not to be feasible. However, beside trace analysis, the newly developed method shows potential for NanoSIMS mercury analysis and imaging to be applied to various samples and association of HgSe clusters to cell organelles seems possible

**Supporting information.** Experimental details for the determination of the total mercury concentration in whale liver. Optical images of whale liver tissue samples (Figure S-1). Mass spectra of the mercury standard and the nanocrystalline HgSe powder after coating with a 5-nm gold layer (Figure S-2). Line scans for estimation of the particle size (Figure S-3).

**Acknowledgments.** The work was supported by funding from the French 'Ministère de l'Enseignement Supérieur et de la Recherche' via the project ANR-11-EQPX-0027 MARSS.

**Conflict of Interest Disclosure.** The authors declare no competing financial interest.

## References

(1) Clarkson, T. W. The Three Modern Faces of Mercury. *Environ. Health Perspect.* **2002**, *110* (SUPPL. 1), 11–23. https://doi.org/10.1289/ehp.02110s111.

(2) Pollman, C. D.; Axelrad, D. M. Mercury Bioaccumulation Factors and Spurious Correlations. *Sci. Total Environ.* **2014**, *496*, vi–xii. https://doi.org/10.1016/j.scitotenv.2014.07.050.

(3) Douglas, T. A.; Loseto, L. L.; MacDonald, R. W.; Outridge, P.; Dommergue, A.; Poulain, A.; Amyot, M.; Barkay, T.; Berg, T.; Chetelat, J.; Constant, P.; Evans, M.; Ferrari, C.; Gantner, N.; Johnson, M. S.; Kirk, J.; Kroer, N.; Larose, C.; Lean, D.; Nielsen, T. G.; Poissant, L.; Rognerud, S.; Skov, H.; Sørensen, S.; Wang, F.; Wilson, S.; Zdanowicz, C. M. The Fate of Mercury in Arctic Terrestrial and Aquatic Ecosystems, a Review. *Environ. Chem.* **2012**, *9* (4), 321–355. https://doi.org/10.1071/EN11140.

(4) MacDonald, R. J.; King, B. V. SIMS — Secondary Ion Mass Spectrometry. In *Surface Analysis Methods in Materials Science*; O'Connor, John, Sexton, Brett, Smart, R. S. C., Ed.; Springer-Verlag Berlin Heidelberg, 2003; pp 127–154. https://doi.org/10.1007/978-3-662-05227-3_5.

(5) Benninghoven, A. Chemical Analysis of Inorganic and Organic Surfaces and Thin Films by Static Time-of-Flight Secondary Ion Mass Spectrometry (TOF-SIMS).

*Angew. Chemie Int. Ed. English* **1994**, *33* (10), 1023–1043. https://doi.org/10.1002/anie.199410231.

(6) Boxer, S. G.; Kraft, M. L.; Weber, P. K. Advances in Imaging Secondary Ion Mass Spectrometry for Biological Samples. *Annu. Rev. Biophys.* **2009**, *38* (1), 53–74. https://doi.org/10.1146/annurev.biophys.050708.133634.

(7) Lechene, C.; Hillion, F.; McMahon, G.; Benson, D.; Kleinfeld, A. M.; Kampf, J. P.; Distel, D.; Luyten, Y.; Bonventre, J.; Hentschel, D.; Park, K. M.; Ito, S.; Schwartz, M.; Benichou, G.; Slodzian, G. High-Resolution Quantitative Imaging of Mammalian and Bacterial Cells Using Stable Isotope Mass Spectrometry. *J. Biol.* **2006**, *5*, 1–30. https://doi.org/10.1186/jbiol42.

(8) Schwarz, S. A. Secondary Ion Mass Spectroscopy. In *Encyclopedia of Materials: Science and Technology*; Jürgen Buschow, K. H., Cahn, R. W., Veyssière, P., et.al., Eds.; Pergamon, 2001; pp 8283–8290. https://doi.org/10.1016/b0-08-043152-6/01482-0.

(9) Storms, H. A.; Brown, K. F.; Stein, J. D. Evaluation of a Cesium Positive Ion Source for Secondary Ion Mass Spectrometry. *Anal. Chem.* **1977**, *49* (13), 2023–2030. https://doi.org/10.1021/ac50021a034.

(10) Vlasov, A. P.; Bonchyk, O. Y.; Kiyak, S. G.; Fodchuk, I. M.; Zaplitnyy, R. M.; Kazemirskiy, T.; Barcz, A.; Zieba, P. S.; Swiatek, Z.; Maziarz, W. Reconstruction of Lattice Structure of Ion-Implanted near-Surface Regions of Hg1 - XCdXTe Epitaxial Layers. *Thin Solid Films* **2008**, *516* (22), 8106–8111. https://doi.org/10.1016/j.tsf.2008.04.075.

(11) Holland, R.; Blackmore, G. W. The Quantitative Application of SIMS to Cadmium Mercury Telluride. *Int. J. Mass Spectrom. Ion Phys.* **1983**, *46*, 527–530.

(12) Battistoni, C.; Bemporad, E.; Galdikas, A.; Kačiulis, S.; Mattogno, G.; Mickevičius, S.;

Olevano, V. Interaction of Mercury Vapour with Thin Films of Gold. *Appl. Surf. Sci.* **1996**, *103* (2), 107–111. https://doi.org/10.1016/0169-4332(96)00518-1.

(13) De Marco, R.; Pejcic, B.; Prince, K.; Van Riessen, A. A Multi-Technique Surface Study of the Mercury(II) Chalcogenide Ion-Selective Electrode in Saline Media. *Analyst* **2003**, *128* (6), 742–749. https://doi.org/10.1039/b212914k.

(14) Sabri, Y. M.; Ippolito, S. J.; Tardio, J.; Atanacio, A. J.; Sood, D. K.; Bhargava, S. K. Mercury Diffusion in Gold and Silver Thin Film Electrodes on Quartz Crystal Microbalance Sensors. *Sensors Actuators, B Chem.* **2009**, *137* (1), 246–252. https://doi.org/10.1016/j.snb.2008.11.032.

(15) Zalavutdinov, R. K.; Dai, Y.; Gorodetsky, A. E.; Bauer, G. S.; Alimov, V. K.; Zakharov, A. P. A Study on Martensitic and Austenitic Steels after Exposure in Mercury at 573 K up to 5000 H. *J. Nucl. Mater.* **2001**, *296* (1–3), 219–224. https://doi.org/10.1016/S0022-3115(01)00546-3.

(16) Nitz, H. M.; Ganschow, O.; Kaiser, U.; Wiedmann, L.; Benninghoven, A. Quasisimultaneous SIMS, AES, XPS, and TDMS Study of Preferential Sputtering, Diffusion, and Mercury Evaporation in CdxHg1-XTe. *Surface Science*. 1981, pp 365–383. https://doi.org/10.1016/0039-6028(81)90066-2.

(17) Groenewold, G. S.; Appelhans, A. D.; Ingram, J. C. Characterization of Bis(Alkylamine)Mercury Cations from Mercury Nitrate Surfaces by Using an Ion Trap Secondary Ion Mass Spectrometer. *J Am Soc Mass Spectrom* **1998**, *9*, 35–41.

(18) Thome, J.; Himmelhaus, M.; Zharnikov, M.; Grunze, M. Increased Lateral Density in Alkanethiolate Films on Gold by Mercury Adsorption. *Langmuir* **1998**, *14* (26), 7435–7449. https://doi.org/10.1021/la9808317.

(19) Nygren, H.; Dahlén, G.; Malmberg, P. Analysis of As- and Hg-Species in Metal-Resistant Oral Bacteria, by Imaging ToF-SIMS. *Basic Clin. Pharmacol. Toxicol.* **2014**,

*115* (1), 129–133. https://doi.org/10.1111/bcpt.12205.

(20) Keune, K.; Boon, J. J. Analytical Imaging Studies Clarifying the Process of the Darkening of Vermilion in Paintings. *Anal. Chem.* **2005**, *77* (15), 4742–4750. https://doi.org/10.1021/ac048158f.

(21) Jaswal, B. B. S.; Kumar, V.; Swart, H. C.; Sharma, J.; Rai, P. K.; Singh, V. K. Multi-Spectroscopic Analysis of Cholesterol Gallstone Using TOF-SIMS, FTIR and UV–Vis Spectroscopy. *Applied Physics B: Lasers and Optics*. 2015, pp 49–56. https://doi.org/10.1007/s00340-015-6200-3.

(22) Malherbe, J.; Penen, F.; Isaure, M. P.; Frank, J.; Hause, G.; Dobritzsch, D.; Gontier, E.; Horréard, F.; Hillion, F.; Schaumlöffel, D. A New Radio Frequency Plasma Oxygen Primary Ion Source on Nano Secondary Ion Mass Spectrometry for Improved Lateral Resolution and Detection of Electropositive Elements at Single Cell Level. *Anal. Chem.* **2016**, *88* (14), 7130–7136. https://doi.org/10.1021/acs.analchem.6b01153.

(23) Bolea-Fernandez, E.; Rua-Ibarz, A.; Krupp, E. M.; Feldmann, J.; Vanhaecke, F. High-Precision Isotopic Analysis Sheds New Light on Mercury Metabolism in Long-Finned Pilot Whales (Globicephala Melas). *Sci. Rep.* **2019**, *9* (1), 1–10. https://doi.org/10.1038/s41598-019-43825-z.

(24) Gajdosechova, Z.; Lawan, M. M.; Urgast, D. S.; Raab, A.; Scheckel, K. G.; Lombi, E.; Kopittke, P. M.; Loeschner, K.; Larsen, E. H.; Woods, G.; Brownlow, A.; Read, F. L.; Feldmann, J.; Krupp, E. M. In Vivo Formation of Natural HgSe Nanoparticles in the Liver and Brain of Pilot Whales. *Sci. Rep.* **2016**, *6* (September), 1–11. https://doi.org/10.1038/srep34361.

(25) Kristl, M.; Drofenik, M. Sonochemical Synthesis of Nanocrystalline Mercury Sulfide, Selenide and Telluride in Aqueous Solutions. *Ultrason. Sonochem.* **2008**, *15* (5), 695–699. https://doi.org/10.1016/j.ultsonch.2008.02.007.

(26) Gao, Y. Influence of Experimental Conditions on Matrix Effect in SIMS. *Appl. Surf. Sci.* **1988**, *32*, 420–430.

(27) Pett-Ridge, J.; Weber, P. K. NanoSIP: NanoSIMS Applications for Microbial Biology. In *Methods in Molecular Biology*; 2012; Vol. 881, pp 375–408. https://doi.org/10.1007/978-1-61779-827-6_13.

(28) Delcorte, A.; Bertrand, P. Interest of Silver and Gold Metallization for Molecular SIMS and SIMS Imaging. *Appl. Surf. Sci.* **2004**, *231–232*, 250–255. https://doi.org/10.1016/j.apsusc.2004.03.029.

(29) Kershaw, J. L.; Hall, A. J. Mercury in Cetaceans: Exposure, Bioaccumulation and Toxicity. *Sci. Total Environ.* **2019**, *694*, 133683. https://doi.org/10.1016/j.scitotenv.2019.133683.

(30) Gajdosechova, Z.; Brownlow, A.; Cottin, N. T.; Fernandes, M.; Read, F. L.; Urgast, D. S.; Raab, A.; Feldmann, J.; Krupp, E. M. Possible Link between Hg and Cd Accumulation in the Brain of Long-Finned Pilot Whales (Globicephala Melas). *Sci. Total Environ.* **2016**, *545–546*, 407–413. https://doi.org/10.1016/j.scitotenv.2015.12.082.

(31) McCormack, M. A.; Fielding, R.; Kiszka, J. J.; Paz, V.; Jackson, B. P.; Bergfelt, D. R.; Dutton, J. Mercury and Selenium Concentrations, and Selenium:Mercury Molar Ratios in Small Cetaceans Taken off St. Vincent, West Indies. *Environ. Res.* **2020**, *181* (September 2019), 108908. https://doi.org/10.1016/j.envres.2019.108908.

(32) Cáceres-Saez, I.; Haro, D.; Blank, O.; Aguayo Lobo, A.; Dougnac, C.; Arredondo, C.; Cappozzo, H. L.; Guevara, S. R. High Status of Mercury and Selenium in False Killer Whales (Pseudorca Crassidens, Owen 1846) Stranded on Southern South America: A Possible Toxicological Concern? *Chemosphere* **2018**, *199*, 637–646. https://doi.org/10.1016/j.chemosphere.2018.02.046.

(33) Nakazawa, E.; Ikemoto, T.; Hokura, A.; Terada, Y.; Kunito, T.; Tanabe, S.; Nakai, I. The Presence of Mercury Selenide in Various Tissues of the Striped Dolphin: Evidence from μ-XRF-XRD and XAFS Analyses. *Metallomics*. 2011, pp 719–725. https://doi.org/10.1039/c0mt00106f.

# SUPPORTING INFORMATION

# Development of mercury analysis by NanoSIMS for the localization of mercury-selenium particles in whale liver

Maria Angels Subirana[1], Lhiam Paton[2], James Hall[3], Andrew Brownlow[4], Eva M. Krupp[3], Jörg Feldmann[2] and Dirk Schaumlöffel[1*]

[1]CNRS, Université de Pau et des Pays de l'Adour, E2S UPPA, Institut des Sciences Analytiques et de Physico-Chimie pour l'Environnement et les Matériaux, UMR 5254, 64000 Pau, France.
dirk.schaumloeffel@univ-pau.fr

[2]TESLA-Analytical Chemistry, Institute of Chemistry, University of Graz, 8010 Graz, Austria

[3]TESLA-Chemistry, School of Computing and Physical Sciences, University of Aberdeen, Aberdeen, AB24 3UE, Scotland, UK

[4]Marine Animal Stranding Scheme, Institute of Biodiversity, Animal Health & Comparative Medicine, College of Medical, Veterinary & Life Sciences, University of Glasgow, Glasgow, G12 8QQ, Scotland, UK

**Table of contents**

**Total mercury analysis in whale liver**

Cold vapour atomic fluorescence spectrometry (PS Analytical Ltd, UK) was used to establish the total Hg concentration in the liver of the sperm whale. 0.1 g of freeze dried, homogenized whale liver samples underwent closed vessel digestion (Mars 5, CEM Corporation, UK). The Millemium Merlin mode of the CV-AFS was used for this analysis. As such, the samples (prepared in 5 % $HNO_3$) were mixed with 5 % $HNO_3$ blank solution before being reduced by 2 % $SnCl_2$ solution. A gas-liquid separator was used to separate the $Hg^0$ vapour and direct it towards the detector this was achieved by purging the solution with Ar gas. DORM-4 and TORT-3 (National Research Council, Canada) certified reference materials were digested and measured in the same manner, giving total recoveries of 81.6 % and 105.2 % respectively. The total Hg concentration in the liver of the sperm whale was 86 mg $kg^{-1}$ dry weight.

**Optical images of whale liver tissue samples**

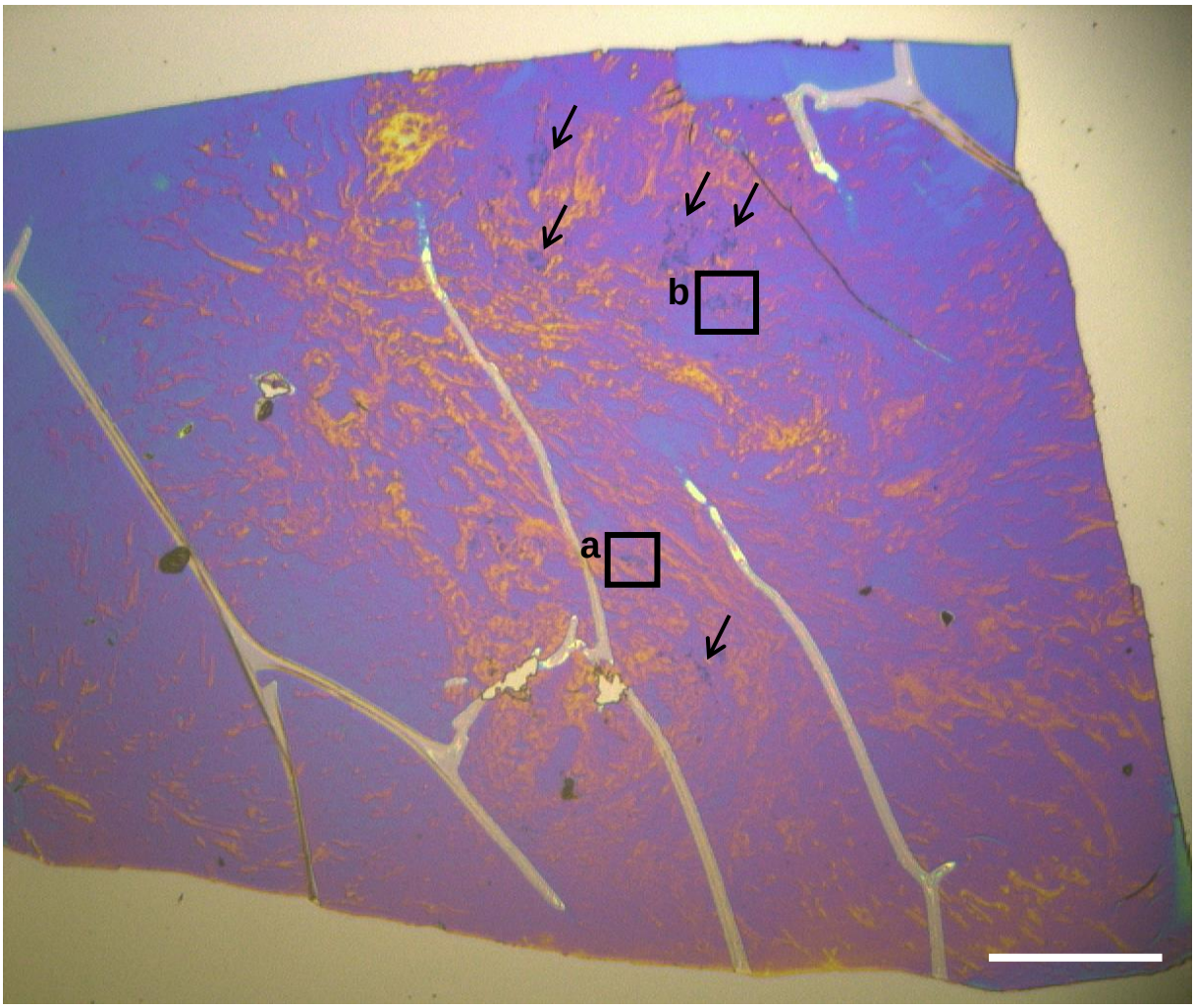


Figure S-1: Optical images of whale liver tissue samples obtained with the build-in CCD camera of the NanoSIMS instruments for selection of areas for NanoSIMS mapping. Black squares indicate areas for NanoSIMS acquisition of Figures 4 a and b, which contain visible darker spots that correspond to HgSe agglomerations. Arrows indicate other HgSe agglomerations present in the liver tissue as an example to illustrate that HgSe is found throughout the tissue. Scale bar is 100 µm.

**Mass spectra of the mercury standard and the nanocrystalline HgSe powder after coating with a 5-nm gold layer**

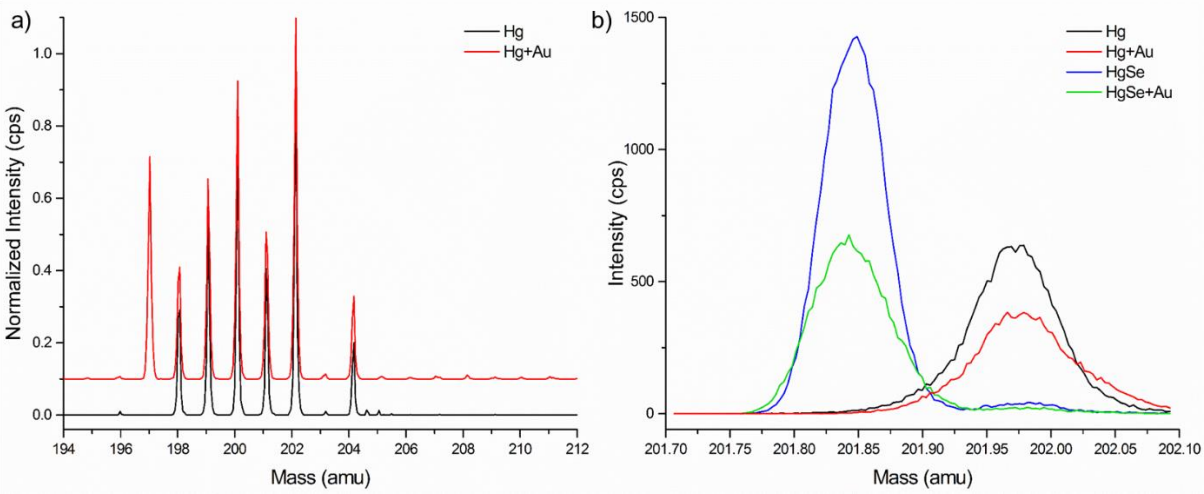


Figure S-2: a) Mass spectrum obtained by a magnetic field scan from a mercury standard (black) and from a 5-nm gold coated mercury standard (red, offset). b) High resolution mass spectra from mass 201.71 to 202.10 obtained from a Hg standard (black), a 5-nm gold coated Hg standard (red), nanocrystalline HgSe (blue), and 5-nm gold coated nanocrystalline HgSe (green).

**Line scans for estimation of the particle size**

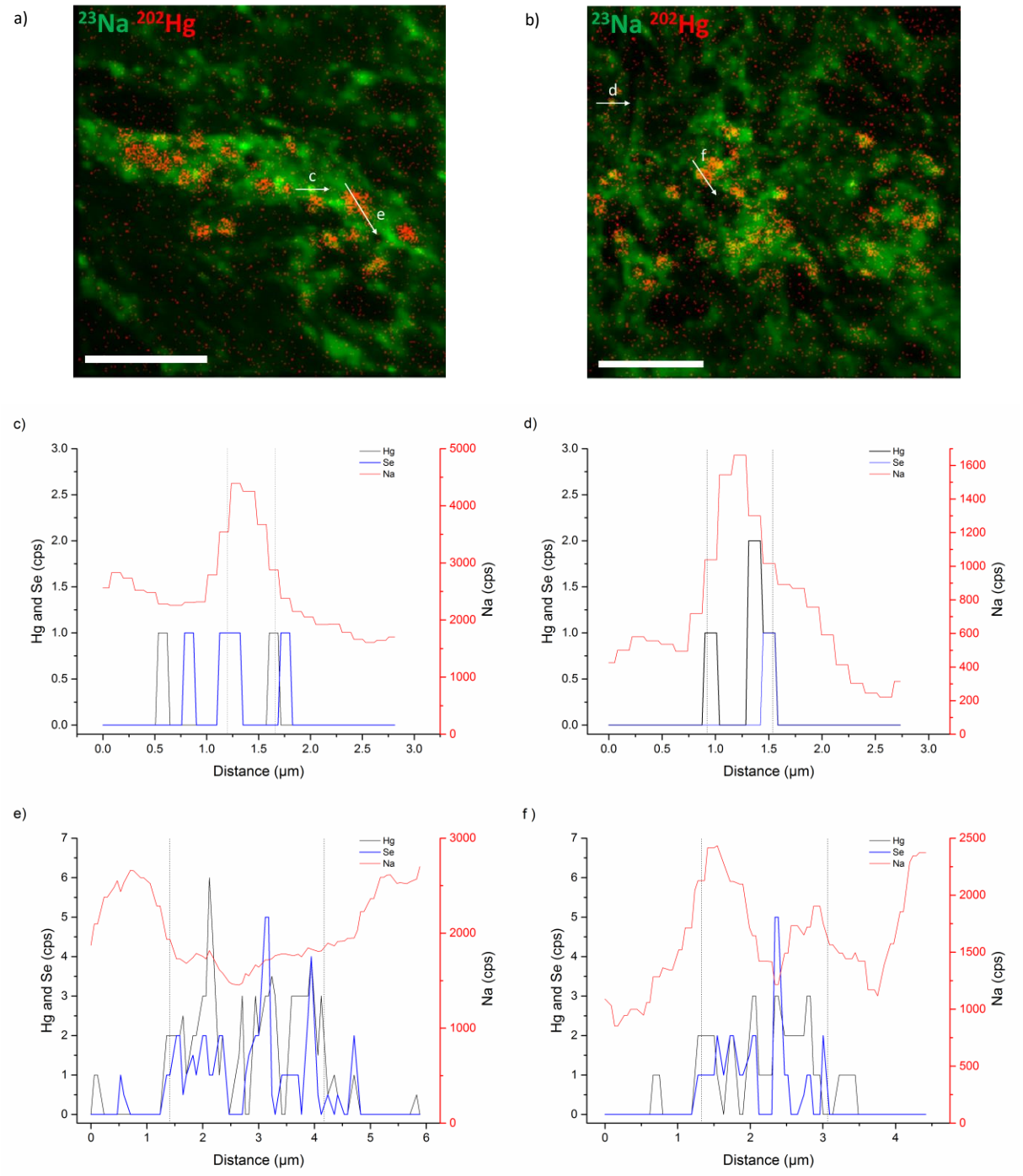


Figure S-3: Line scans through HgSe particles for estimation of the particle size. a) color overlay image of $^{202}$Hg (red) and $^{23}$Na (green) from Figure 4a, where white arrows indicate the line scans in c and e. b) color overlay image of $^{202}$Hg (red) and $^{23}$Na (green) from Figure 4b, where white arrows indicate the line scans in c and e. c), d), e) and f) line scans in the respective arrow position of $^{202}$Hg (black) and $^{80}$Se (blue) in the left vertical axis and $^{23}$Na (red) in the right vertical axis. Scale bar is 10 µm.